Nanoscale

Cite this: *Nanoscale*, 2011, **3**, 3700

www.rsc.org/nanoscale

PAPER

In situ transmission electron microscopy of solid–liquid phase transition of silica encapsulated bismuth nanoparticles

Jianjun Hu,*[ac] Yan Hong,[b] Chris Muratore,[c] Ming Su[b] and Andrey A. Voevodin[c]

Received 18th April 2011, Accepted 5th June 2011
DOI: 10.1039/c1nr10394f

The solid–liquid phase transition of silica encapsulated bismuth nanoparticles was studied by *in situ* transmission electron microscopy (TEM). The nanoparticles were prepared by a two-step chemical synthesis process involving thermal decomposition of organometallic precursors for nucleating bismuth and a sol–gel process for growing silica. The microstructural and chemical analyses of the nanoparticles were performed using high-resolution TEM, Z-contrast imaging, focused ion beam milling, and X-ray energy dispersive spectroscopy. Solid–liquid–solid phase transitions of the nanoparticles were directly recorded by electron diffractions and TEM images. The silica encapsulation of the nanoparticles prevented agglomeration and allowed particles to preserve their original volume upon melting, which is desirable for applications of phase change nanoparticles with consistently repeatable thermal properties.

Introduction

Phase change material (PCM) can absorb and release a significant amount of heat during solid–liquid–solid phase transitions.[1] Dissipating thermal energy into PCMs results in an isothermal process for transferring heat. Various PCMs have been studied for thermal energy storage and heat transfer applications.[2–5] The size effects at the nanoscale on melting point depression and isothermal heat absorption are well-known,[6] however the effects of nucleation at the nanoscale are not as widely reported, but are significant for the use of nanoparticle PCMs for thermal management, as investigated here. In addition, encapsulation of PCMs had been proposed to prevent their agglomeration and leakage upon melting that could result in variable thermal properties in the following melting–solidifying cycles.[2] Dielectric encapsulation of PCM nanoparticles in heat transfer fluids was required for cooling high-power-density-electronic circuits with novel microchannel heat sinks.[5] Although metallic nanoparticles are often produced by the colloidal method[7–9] and encapsulated by the sol–gel process,[10–12] there were limited reports on encapsulation and studies of PCM nanoparticles of low-melting-point metals. Recently, we proposed the application of encapsulated PCM nanoparticles for increasing the heat capacity of a colloidal suspension at a specific temperature to transfer heat,[13] and for nano-heat-sinks in the thermal management of heterogeneous chemical reactions.[14] However, there is still interest in investigating the microstructural changes of PCM nanoparticles at melting temperatures.

Transmission electron microscopy (TEM) is a common technique to study the microstructure of static materials with high-spatial resolution. Information on the real-time response of microstructures to changes in temperature is useful for the investigation of PCM nanoparticles because their properties strongly depend on their temperature-dependent microstructures. *In situ* TEM techniques have proved to be useful methods for direct measurement of thermodynamically driven changes in microstructure with increasing temperatures.[15,16] In this paper, we focus on phenomena observed during annealing of bare and silica-encapsulated bismuth nanoparticles in a TEM. Bismuth has a melting temperature of 271.5 °C, which is higher than indium (156.60 °C) but lower than lead (327.46 °C). Bismuth is known for its highly anisotropic Fermi surface, long Fermi wavelength and mean-free path of carriers. A strong quantum finite-size effect has been examined in nanoscale bismuth particles.[17] Silica encapsulation was applied to contain the metallic core upon melting and was chosen because of its excellent stability at high temperatures.[18] The results show the benefits of silica-encapsulation of bismuth nanoparticles for prevention of agglomeration and leakage upon melting. Such experiments have not been reported in detail or employed in PCM nanoparticle investigations before.

Experimental details

Bismuth acetate, tetraethoxysilane (TEOS), poly-vinyl-pyrrolidone (PVP), ammonium hydroxide (NH_4OH) and

[a]*University of Dayton Research Institute, Dayton, Ohio, 45469, USA. E-mail: Jianjun.Hu@WPAFB.AF.MIL; Fax: +1 937 2552176; Tel: +1 937 2559073*
[b]*NanoScience Technology Center, University of Central Florida, Orlando, Florida, 32826, USA*
[c]*Materials and Manufacturing Directorate, Air Force Research Laboratory (AFRL/RXBT), Wright-Patterson Air Force Base, Bldg. 654, 2941 Hobson Way, Room 10, Dayton, Ohio, 45433-7750, USA*

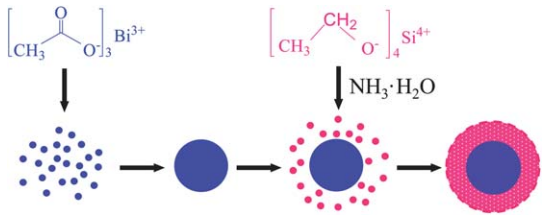

Fig. 1 Illustration of synthesis and encapsulation of silica-encapsulated bismuth nanoparticles.

ethylene glycol were obtained from Aldrich. Fig. 1 shows a schematic diagram of making silica encapsulated bismuth nanoparticles, where bismuth cores were grown by thermal decomposition of organometallic precursors and then encapsulated with silica shells by a sol–gel method. PVP was added as a protective agent. Briefly, 1.5 mmol of bismuth acetate with 0.2 g of PVP was added into a vigorously stirred reaction vessel that contained 20 mL of ethylene glycol at 200 °C under dry nitrogen. After reacting for 20 minutes, the reaction was quenched by pouring the hot mixture into 200 mL of ethanol that was pre-cooled to 0 °C. The nanoparticles were purified by centrifuging at 4000 rpm for 10 minutes and washing by ethanol (90%) for three times. After re-suspending 50 mg of bismuth nanoparticles into 50 mL of ethanol, 2 mL of NH_4OH (concentration of 28%) and 0.2 mL of TEOS were added drop-wise into the solution, which was sonicated at 70 °C for 1.5 hours to decompose TEOS and form silica shells on the nanoparticles. After the reaction, the mixture was centrifuged to remove the top clear solution and then washed with ethanol for three times. Both the bare and encapsulated nanoparticle samples were then prepared for microstructural, thermal and *in situ* TEM characterizations.

A JEOL6400 field-emission-gun scanning electron microscope (SEM) was used to take images at an acceleration voltage of 10.0 kV. The samples for SEM measurements were prepared by depositing small drops of nanoparticle suspension on silicon substrates. XRD spectra were recorded using a Rigaku 2500 diffractometer with a monochromator in front of the Cu K_α X-ray source (40.0 kV and 30.0 mA) at a step width of 2.0° min^{-1}. The nanoparticle powders were glued onto a double side tape that was mounted on a XRD specimen holder. Standard powder XRD patterns were used for data interpretation.

Isothermal heat absorption and release of the phase change nanoparticles were studied using a PerkinElmer differential scanning calorimeter (DSC). Approximately 10.0 mg of bismuth

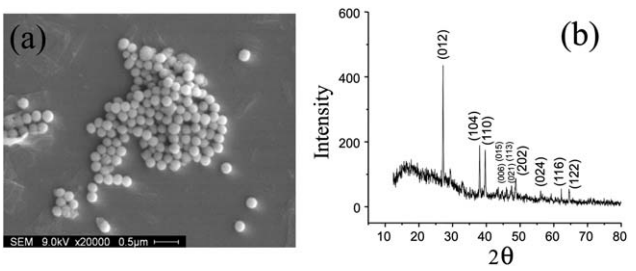

Fig. 2 (a) Scanning electron microscope image of bismuth nanoparticles deposited on silicon wafer. (b) X-Ray diffraction spectrum of bismuth nanoparticles.

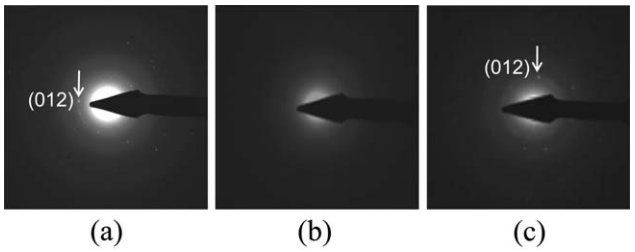

Fig. 3 Electron diffraction patterns taken from bismuth nanoparticles at a temperature of (a) approximately 23 °C, (b) 272 °C, and (c) 167 °C, respectively, by *in situ* transmission electron microscopy.

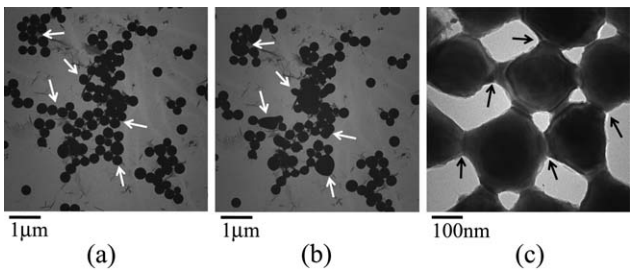

Fig. 4 *In situ* TEM images taken from (a) as-synthesized bismuth nanoparticles, (b) the bismuth nanoparticles after annealing, and (c) the sintering necks formed between bismuth nanoparticles after annealing.

nanoparticles was hermetically sealed in an aluminium pan and placed in the DSC chamber, which was purged continuously by nitrogen gas. Dynamic scans were carried out at a heating rate of 2 °C min^{-1} from room temperature to 300 °C. The reversible phase change of bismuth nanoparticles was measured when temperature was increased and decreased. The melting and solidification peaks of the nanoparticles were determined at 271.5 °C and 167.2 °C, respectively, which indicated a large super-cooling due to the homogeneous nucleation of molten bismuth nanoparticles. Although the bismuth materials are surrounded by silica that can plausibly act as a nucleation site, their interface is smooth and the contact angle is large based on interfacial energy calculations. Therefore, molten bismuth does not wet and nucleation is homogeneous rather than heterogeneous. A method to reduce super-cooling had recently been proposed by encapsulating with the silica shells of rough interface and small contact angle derived from water glass.[19]

TEM specimens were prepared by dispersing a drop of nanoparticle suspension on 200 mesh copper grids coated with

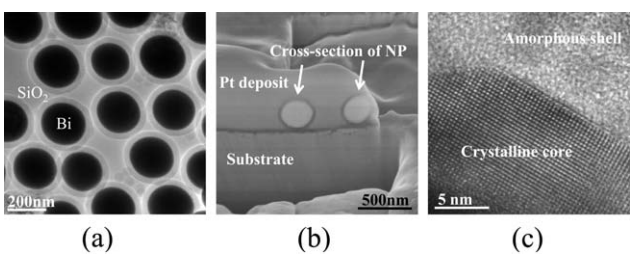

Fig. 5 (a) TEM image taken from silica-encapsulated bismuth nanoparticles; (b) cross-sectional image of silica-encapsulated bismuth nanoparticles performed in a FIB microscope; (c) high-resolution TEM image taken at the interface between silica shell and bismuth core.

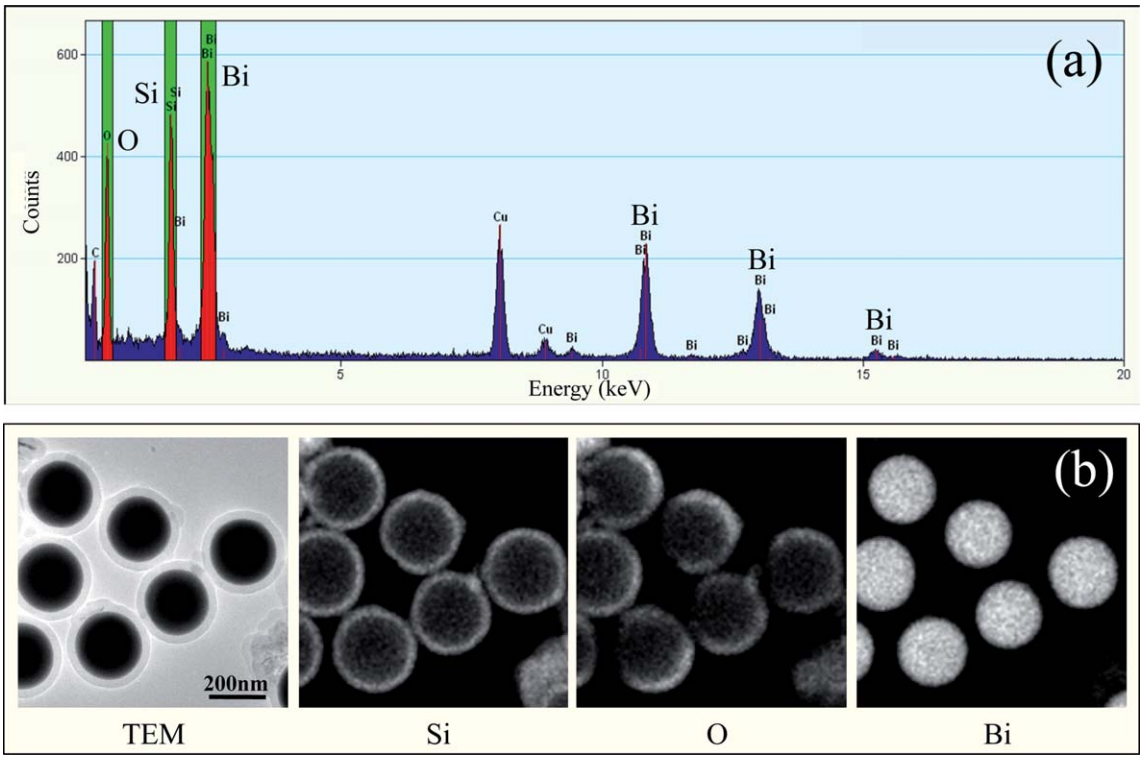

Fig. 6 (a) X-Ray energy dispersive spectrum collected from silica-encapsulated bismuth nanoparticles, where the energy peaks of elements Si, O and Bi were indicated. (b) TEM image taken from silica-encapsulated bismuth nanoparticles and the corresponding EDS elemental mapping results for Si, O and Bi, respectively.

carbon films. *In situ* TEM annealing of specimens was performed by using a Gatan 652 double tilt heating holder with a Gatan model 628 power supply (maximum operating temperature up to 1000 °C), which was inserted into a Philips CM200 LaB_6 TEM operated at 200 kV. The reading temperatures were calibrated by using thermocouple wires welded to a specimen through the heating range. Dynamic TEM images and electron diffractions during heating and cooling processes were recorded using a charge-coupled device (CCD) camera and synchronously saved in digital video files. High-resolution microstructure and chemistries of the nanoparticles were measured using a FEI Titan™ 80-300 S/TEM, associated with an X-ray energy dispersive spectroscopy (EDS) detector for elemental mapping and a high-angle annular dark-field (HAADF) detector for Z-contrast imaging. In addition, a FEI-DB235 focused ion beam (FIB) microscope equipped with an Omniprobe manipulator was used to prepare TEM specimens in order to analyze the cross-sectional microstructure of the nanoparticles. The FIB microscope was operated with 5 kV electron beams and 30 kV Ga^+ ion beams. To protect nanoparticle surfaces from incident ion beam bombardment, a platinum protection cap of approximately 2 μm thickness was deposited on the top of sample surfaces using a gas injection system by ion beam patterning at a moderate low current of 100 pA.

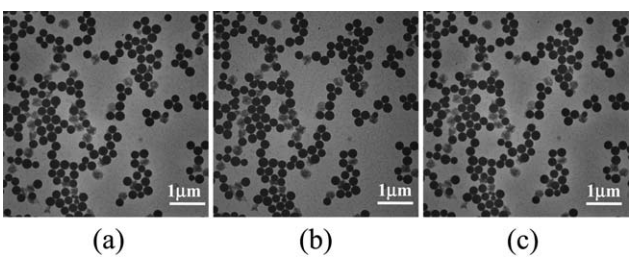

Fig. 7 *In situ* TEM images taken from silica-encapsulated bismuth nanoparticles (a) before annealing, (b) at approximately 300 °C, and (c) after solidifying.

Results and discussion

The SEM image shows that the granular bismuth nanoparticles have a uniform diameter of approximately 200 nm, as shown in Fig. 2(a). The XRD spectrum recorded for the nanoparticles exhibits strong rhombohedral peaks as indexed with a standard diffraction pattern (JCPDS Powder Diffraction File, *i.e.*, PDF Card#44-1246), as shown in Fig. 2(b). Some weak diffraction peaks could result from the slight oxide formation when the bismuth nanoparticles were measured in air. The DSC measurements show that bismuth nanoparticles melt at 271.5 °C, which is in good agreement with bismuth crystals. Furthermore, the solid–liquid phase transition of bismuth nanoparticles was studied by *in situ* TEM. Fig. 3(a and b) show the electron diffraction patterns recorded during the heating process and Fig. 3(b and c), the cooling process, respectively. They were taken from a selected area of 5 μm diameter, which included dozens of bismuth nanoparticles. The electron diffraction spots from crystalline nanoparticles disappeared at approximately 272 °C, as shown in Fig. 3(b), indicating a solid-to-liquid phase transition

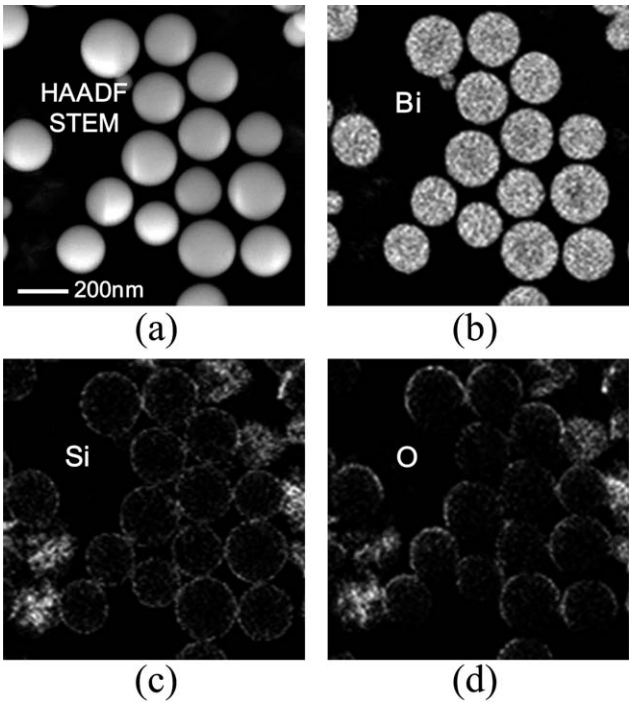

Fig. 8 (a) HAADF-STEM image taken from silica-encapsulated bismuth nanoparticles after *in situ* TEM annealing, and the corresponding EDS elemental mapping results for (b) Bi, (c) Si, and (d) O, respectively.

of bismuth. Solidification of the nanoparticles was not observed until the temperature decreased to approximately 167 °C (Fig. 3 (c)). This solidifying temperature is much lower than the melting point of the nanoparticles, consistent with our previous DSC measurements. This observed super-cooling could be caused by homogeneous nucleation of bismuth nanoparticles because of the expected increased nucleation barrier compared to heterogeneous nucleation. *In situ* TEM images were taken from as-made bismuth nanoparticles (Fig. 4(a)), and compared with the same observation area after annealing (Fig. 4(b)), where the agglomeration of bismuth nanoparticles after melting is indicated by white arrows. Fig. 4(c) further reveals the formation of neck-like connections among bismuth nanoparticles as indicated by black arrows in the image. Without a diffusion barrier, bismuth nanoparticles sinter and agglomerate with increasing temperatures.

Silica has high melting temperature (approximately 1650 °C), excellent thermal and chemical stability, thermal shock resistance, oxidation protection, and high dielectric constant. Conformal silica shells show a relatively bright contrast compared to that of bismuth cores, as shown in Fig. 5(a). Fig. 5 (b) shows the cross-sectional image of the nanoparticles taken in a FIB microscope. High-resolution TEM image reveals the bismuth cores of a crystalline phase and the silica shells of an amorphous phase, as shown in Fig. 5(c), which is consistent with our XRD measurements. The chemical compositions of the nanoparticles were measured by EDS analyses. Bi, Si and O characteristic peaks were identified on the EDS spectrum, as shown in Fig. 6(a), where the Cu and C signals came from a carbon-coated-copper TEM grid for supporting the samples. Fig. 6(b) shows the EDS elemental mapping results from the silica shell (composed of Si and O) and bismuth core, respectively, in corresponding to the TEM image provided on the left. It is demonstrated that the produced silica-encapsulated bismuth nanoparticles are quite uniform in the shell thickness, core size and geometry.

Fig. 7 shows *in situ* TEM images taken from the silica-encapsulated bismuth nanoparticles: (a) before annealing, (b) at approximately 300 °C, and (c) after solidifying, where no remarkable morphological change has been found between the nanoparticles before and after annealing. The encapsulated nanoparticles demonstrated a high thermal stability while the bare nanoparticles exhibited significant agglomeration during a similar *in situ* TEM annealing process. The annealed nanoparticles were then studied by using a Z-contrast imaging technique. Fig. 8(a) shows a HAADF-STEM image taken after *in situ* TEM annealing, where spherical bismuth cores are clearly shown

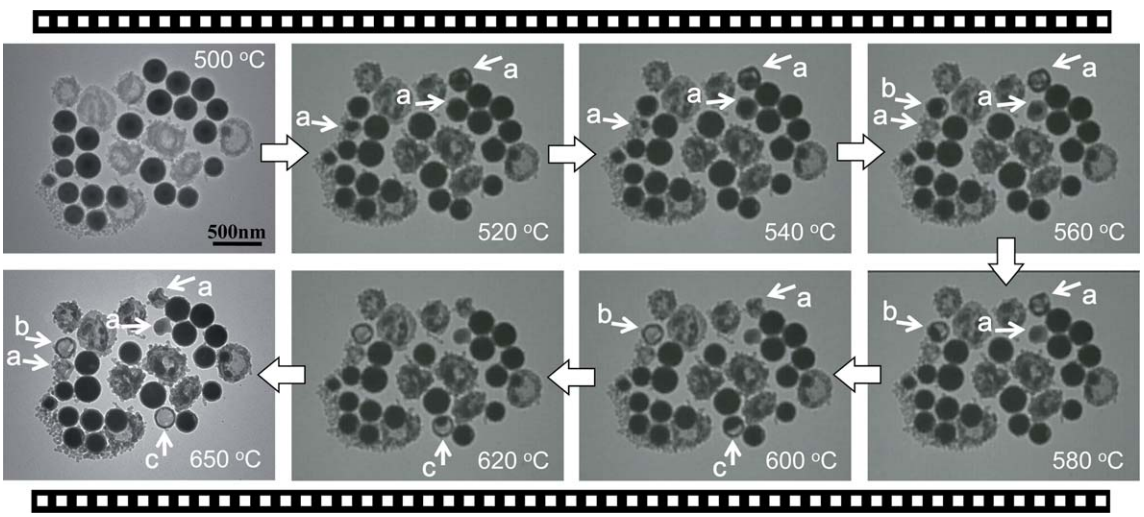

Fig. 9 A series of *in situ* TEM images recorded from silica-encapsulated bismuth nanoparticles, where some leakages of bismuth core materials were indicated with arrows "a", "b" and "c".

with bright contrast due to the high atomic mass of bismuth. The chemistry of the annealed nanoparticles was also measured by EDS elemental mapping for bismuth, silicon and oxygen, respectively, as shown in Fig. 8(b, c and d). No evidence of agglomeration, leakage or oxidation of nanoparticles was found during these *in situ* TEM experiments at temperatures up to 300 °C. Thus, the bismuth core materials were well preserved by the silica shells during solid–liquid phase transitions.

Moderate leakage of bismuth core materials was observed when the temperature was increased higher than 500 °C. Fig. 9 shows *in situ* TEM images taken from silica-encapsulated bismuth nanoparticles when heating from approximately 500 °C to 650 °C, by recording with a CCD camera. At high temperatures, some silica shells collapsed after losing the bismuth core materials as indicated by arrows "a" in Fig. 9. Those could be the silica shells with some defects, which were susceptible to deformation or breakage, leaking first at temperatures above 500 °C. As the temperature increased, the silica shells with fewer defects started to leak bismuth materials, as indicated by arrows "b" and "c" in Fig. 9. In particular, the silica shell indicated by arrow "c" maintained its spherical shape after losing its core material. These results imply that the structure of the silica shells dictates the magnitude of maximum acceptable thermal stress during heating. Actually, Fig. 9 shows a large number of the nanoparticles that are not leaking bismuth materials even at 650 °C –suggesting they are protected hermetically by the high quality silica shells with a high thermal stability. Therefore, the silica encapsulation can be used to develop the application of PCM nanoparticles for use in a broad range of high temperatures.

Conclusions

1. Silica encapsulated PCM nanoparticles with desired structures and properties were synthesized by the two-step colloidal method that involved bismuth core formation and silica shell encapsulation. The nanoparticle cores were composed of rhombohedral bismuth with a melting point of 271.5 °C.

2. *In situ* TEM measurements revealed that agglomeration and sintering occurred in bare bismuth nanoparticles after annealing. However, no agglomeration, leakage or oxidation of bismuth core materials was found in the measurements of silica-encapsulated bismuth nanoparticles when increasing temperatures above the melting point of 271.5 °C up to 300 °C.

3. The silica shells demonstrated excellent sealing capability and thermal stability. No agglomeration was formed in the silica-encapsulated nanoparticles even though some of them exhibited to lose bismuth core materials at high temperatures above 500 °C, which was connected to possible defect presence in some of the shells. A large number of the nanoparticles did not leak liquid bismuth core materials after annealing to approximately 650 °C.

4. The microstructure and chemistry of silica-encapsulated bismuth nanoparticles were well preserved during solid–liquid–solid phase transitions upon heating and cooling. They have great potential to provide a consistent performance by preventing agglomeration, leakage and oxidation of PCM nanoparticles in thermal energy capturing and storing required for thermal management applications.

Acknowledgements

The Air Force Office of Scientific Research (AFOSR) is gratefully acknowledged for financial support, and Dr R. Wheeler and S. Apt of UES, Inc. (Microstructure Characterization Facility at AFRL/RX) are thankfully acknowledged for assisting on TEM and FIB experiments.

References

1 B. Zalba, J. M. Marin, L. F. Cabez and H. Mehling, *Appl. Therm. Eng.*, 2003, **23**, 251.
2 M. N. A. Hawlader, M. S. Uddin and H. J. Zhu, *Int. J. Energy Res.*, 2002, **26**, 159.
3 E. Hisham, E.-D. Hisham and A.-K. Eman, *Ind. Eng. Chem. Res.*, 2004, **43**, 5350.
4 M. Kenisarin and K. Mahkamov, *Renewable Sustainable Energy Rev.*, 2007, **11**, 1913.
5 S. Kuravi, K. M. Kota, J. Du and L. C. Chow, *J. Heat Transfer*, 2009, **131**, 062901.
6 Q. Jiang, H. X. Shi and M. Zhao, *J. Chem. Phys.*, 1999, **111**, 2176.
7 N. H. Chow, X. Ke, P. Schiffer and R. E. Schaak, *J. Am. Chem. Soc.*, 2008, **130**, 8140.
8 Y. G. Sun and Y. N. Xia, *Science*, 2002, **13**, 2176.
9 Y. Zhao, Z. Zhang and H. Dang, *J. Phys. Chem. B*, 2003, **107**, 7574.
10 S. H. Joo, J. Y. Park, C.-K. Tsung, Y. Yamada, P. Yang and G. A. Somorjai, *Nat. Mater.*, 2009, **8**, 126.
11 C. Graf, D. L. J. Vossen, A. Imhof and A. V. Blaaderen, *Langmuir*, 2003, **19**, 6693.
12 L. M. Liz-Marzan, M. Giersig and P. Mulvaney, *Langmuir*, 1996, **12**, 4329.
13 Y. Hong, S. Ding, W. Wu, J. Hu, A. A. Voevodin, L. Gschwender, Ed. Snyder, L. Chow and M. Su, *ACS Appl. Mater. Interfaces*, 2010, **2**, 1685.
14 M. Zhang, Y. Hong, S. Ding, J. Hu, Y. Fan, A. A. Voevodin and M. Su, *Nanoscale*, 2010, **2**, 2790.
15 R. Sinclair and T. J. Konno, *Ultramicroscopy*, 1994, **56**, 225.
16 J. J. Hu, A. A. Voevodin and J. S. Zabinski, *Microsc. Microanal.*, 2001, **7**(suppl. 2), 1232, (Proc. Microscopy and Microanalysis, Long Beach, California, 2001).
17 K. Liu, C. L. Chien and P. C. Searson, *Phys. Rev. B: Condens. Matter Mater. Phys.*, 1998, **58**, R14681.
18 C. Radloff and N. J. Halas, *Appl. Phys. Lett.*, 2001, **79**, 674.
19 Y. Hong, W. Wu, J. Hu, M. Zhang, A. A. Voevodin, L. Chow and M. Su, *Chem. Phys. Lett.*, 2011, **504**, 180.

